VALIDATION OF A FINITE ELEMENT MODEL FOR FRACTURE MECHANICS SPECIMENS

J. Maelfait[1], M. Cauwelier[1], M. Verstraete[2], S. Hertelé[2], K. Van Minnebruggen[2] and W. De Waele[2]

[1] Ghent University, Belgium

[2] Ghent University, Laboratory Soete, Belgium

Abstract Single parameter formulations have shown to be insufficient to describe constraint effects in fracture mechanics specimens. This has lead researchers to a two parameter approach like the J-Q theory. In order to investigate constraint effects, the authors have developed a generic finite element model. Prior to drawing conclusions this model must first be validated, which is the topic of this paper. This validation has been done by comparing analytical expressions of the J-integral with those obtained from the performed simulations. The compared geometries were center cracked tension (CCT) and double edge notched tension (DENT) fracture mechanics specimens. The results showed good agreement with the analytical expressions and, as such, the model can now be confidently applied to determine values of the J-integral. This is a first step towards evaluating two parameter J-Q constraint.

Keywords: finite element model, center cracked tension (CCT), double edge notched tension (DENT)

1 INTRODUCTION

In small scale yielding conditions, a single crack driving force parameter (e.g. K, J or CTOD) is sufficient to accurately describe crack tip conditions and as such can be used as a geometry independent fracture criterion. Under large scale yielding conditions, a single parameter is however inadequate. Such condition is no longer geometry independent and therefore another approach is needed. Two parameter fracture mechanics (e.g. T-stress, J-Q theory) offers a solution to this problem. These two parameter approaches allow characterising the different levels of constraint seen in fracture mechanics specimens of different geometries. To study these influences the authors have designed a finite element model. To be able to draw valid conclusions from the simulations a model validation imposes itself.

This paper provides a model validation by comparing its simulated J-integral values with those obtained from published analytical solutions. This is done for both center cracked tension (CCT) and double edge notched tension (DENT) specimen geometries. These geometries are commonly reported in literature and illustrated in Figure 1. Figure 1 also shows the definition of the used geometric parameters: specimen length L, thickness B, width $2W$ and crack depth a. These parameters lead to a number of non-dimensional groups: a/W, L/W and $B/2W$. The relative length L/W will be kept at a constant value of 10 in all analyses for both CCT and DENT, whilst the relative thickness $B/2W$ will be varied and the relative crack depth a/W shall be studied for three discrete values of 0.25, 0.50 and 0.75.

The choice for CCT and DENT geometries was influenced by the availability of analytical expressions and their significance in literature and experimental work. This choice also allows comparing relatively low constraint conditions in the CCT specimen versus the relatively high constraint in a deeply cracked DENT specimen [1].

In literature DENT specimens for example have been used for creep-fatigue tests, tests on metal foams, asphalt binders and polymers [2]. DENT tests are also performed to determine the specific essential work of fracture [3]. A CCT specimen on the other hand is commonly used for the validation of finite element models because of its known analytical solutions [4-6], and in creep crack growth testing [7].

Sometimes side grooves are added to fracture mechanics specimens. The intention of these side grooves is to reduce the tunnelling effect that is often seen during crack growth. Tunneling causes difficulties to unambiguously determine and quantify the crack extension as it is no longer uniform across the specimen thickness. Side grooves also ensure crack growth along a straight path, which might be necessary to achieve accurate measurements depending on the instrumentation used. In [7] a thickness reduction of 20% is suggested for both CCT and DENT. Side grooves are less often employed for CCT specimens and some authors even disadvise them [8].

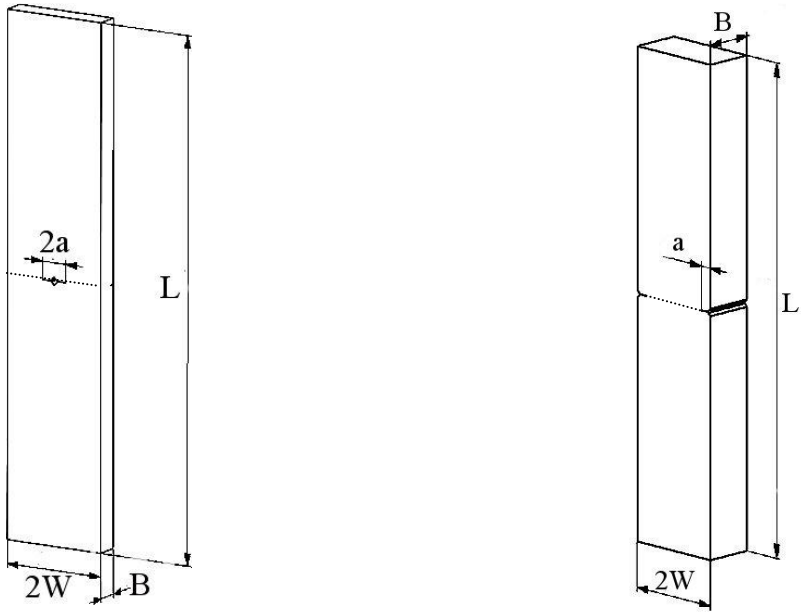

a) b)

Figure 1. a) Center cracked tension (CCT) and b) double edge notched tension (DENT) geometries (location sidegrooves indicated with dashed line)

2 FINITE ELEMENT MODEL

The finite element model was designed for rectangular geometries in which a notch is present. The model was written in Pythoncode for ABAQUS® (version 6.10). The Pythoncode represents a fully parametric script, which allows the user to easily modify the dimensions of the evaluated specimen and the applied notch depth without having to use the graphic user interface. The script also enables the use of different test specimens and allows changing mesh parameters. Adding side grooves is another possibility which is implemented through a nodal coordinate transformation of the meshed geometry. The generic model uses default a single edge notched tension (SENT) specimen as a basis. This base geometry can be mirrored, by applying an appropriate boundary condition, to achieve the DENT or the CCT specimen geometry. By mirroring about the plane opposite to the notch, a DENT specimen is found. This is demonstrated in Figure 2 wherein a DENT geometry is achieved by mirroring the SENT geometry about the YZ plane. One can also deduce from the figure that the SENT geometry itself is produced by mirroring half of the SENT geometry about the XZ plane. By doing so only a quarter of the 3D geometry needs to be analysed, thus significantly reducing processing time without sacrificing accuracy. CCT geometries are analysed in a similar way, by mirroring the SENT geometry about the notched plane.

In addition to 3D calculations, the script also offers the option to conduct a 3D plane strain analysis. This is achieved by applying an extra symmetry boundary condition at the outer plane of the model, parallel to the XZ plane in Figure 2.

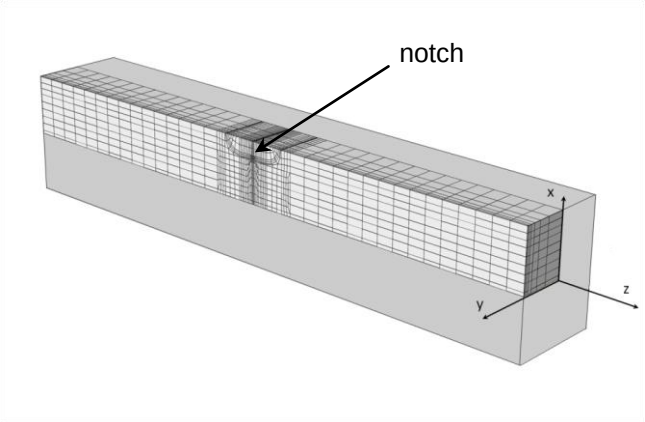

Figure 2. Mirroring about the XZ and YZ or notched plane allows DENT or CCT geometry

2.1 Boundary conditions at the end planes

The finite element model allows for two different types of boundary conditions. The first setting is where the specimens are clamped at their end planes to administer the tensile force. This boundary condition is achieved by applying a constant displacement on one of the end planes (perpendicular to the length, z-axis, keeping the other degrees of freedom fixed) while all degrees of freedom at the other end plane are fixed. The second setting is where the specimen is loaded under tension by being pinned. This allows for small rotations of the specimen. This boundary condition was simulated by the use of a multipoint constraint (MPC) on the end planes of the specimens. In both conditions a displacement is applied instead of a load, which facilitates numerical convergence.

2.2 Mesh parameters

The mesh mostly consists of coarse bricks with a rectangular shape, except for the region close to the crack tip as can be seen in Figure 3b. At the crack tip the mesh assumes a spider web like pattern, which is composed of smaller elements. These smaller elements improve the accuracy of the calculations of the high stress and strain field gradients at the crack tip. This pattern can be discerned in Figure 3c. The amount of elements has been chosen carefully to balance the increase in calculation time and the higher accuracy of the calculation that come with a larger amount of elements. First order linear elements with reduced integration were used (type C3D8R in ABAQUS®).

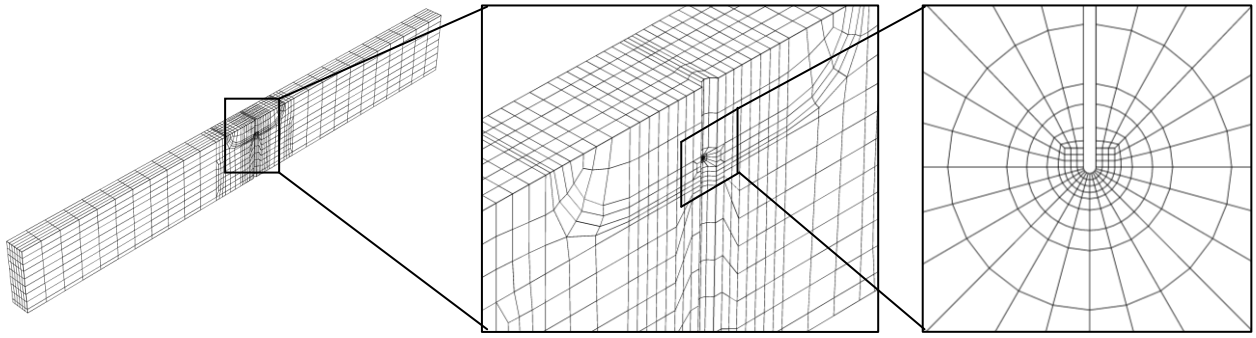

a) b) c)

Figure 3. a) Global view of the mesh for a half SENT specimen with side grooves, b) Detail of crack area with side grooves, c) Spider web mesh at the crack tip

2.3 Material definition

The material model used for the finite element and analytical calculations, was a Ramberg-Osgood type steel. The stress-strain relation can be found in equation (1).

$$\epsilon = \frac{\sigma}{E} + \alpha \frac{\sigma_0}{E} \left(\frac{\sigma}{\sigma_0} \right)^n \tag{1}$$

The yield strength σ_0 is 420 MPa and the Young's modulus equals 210000 MPa. For a nominal yield offset ($\alpha \frac{\sigma_0}{E}$) of 0.002 (which implies that σ_0 represents the 0.2% proof stress), the value of α is equal to 1. The strain hardening coefficient n was chosen to be 10 to account for the steel types which were commonly used at the time these analytical formulas were composed (1981). A small strain analysis was performed, assuming isotropic hardening according to the Von Mises yield criterion.

2.4 Post-processing

In the post-processing stage of the analysis values for the J-integral are determined at the symmetry plane of the SENT geometry (XZ plane in Figure 2). Reaction forces at the MPC's are determined as well and doubled due to symmetry, thus yielding a J versus applied load curve. Load versus crack mouth opening displacement (CMOD) curves can also be constructed, as the CMOD value is also extracted during post-processing.

3 ANALYTICAL FRAMEWORK

Analytical crack driving force solutions have been used to validate the model. These solutions have been found in the EPRI handbook (Kumar et al. [9]) and from Lei et al. [10] and Faucher [11]. Different solutions are available for plane strain and plane stress. The comparison of the finite element simulations and the analytical solutions relies on the proper calculation of elastic and plastic J-integral, to obtain the total J-integral:

$$J = J_{el} + J_{pl} \tag{2}$$

The elastic part is calculated from the stress intensity factor K_I, which can be found in tabulated form as a function of the (normalized) crack depth [12]. P is the applied tensile force.

$$f\left(\frac{a}{W}\right) = \frac{K_I B\sqrt{W}}{P} \tag{3}$$

$$J_{el} = \frac{K_I^2}{E'} \tag{4}$$

E' is the modified Young's modulus, equal to E for plane stress and $E/(1\text{-}\nu^2)$ for plane strain (ν is Poisson's ratio). The plastic part of the J-integral is also dependent on plane strain or plane stress conditions, and has been calculated according to the formulation of the EPRI handbook [9] (Eq. 5). The difference in calculation between plane strain and plane stress lies in different tabulated values of the function h_1 and the use of a different reference load P_0. The function h_1 is dependent on the crack depth and the strain hardening coefficient. Besides the different values of h_1 and P_0, the equation for J_{pl} is the same for plane strain and plane stress.

$$J_{pl} = a\epsilon_0\sigma_0 \frac{ba}{W} h_1\left(\frac{a}{W}, n\right)\left(\frac{P}{P_0}\right)^{n+1} \tag{5}$$

In which b is half the length of the unnotched ligament for both specimen geometries. P_0 is the reference load and is defined as follows.

For CCT specimens:

Plane strain
$$P_0 = \frac{4}{\sqrt{3}} Bb\sigma_0 \tag{6}$$

Plane stress
$$P_0 = 2Bb\sigma_0 \tag{7}$$

For DENT specimens:

Plane strain
$$P_0 = \left(0.72 + 1.82\frac{b}{W}\right) Bb\sigma_0 \tag{8}$$

Plane stress
$$P_0 = \frac{4}{\sqrt{3}} Bb\sigma_0 \tag{9}$$

The tabulated values for f and h_1 are given for a normalized crack depth of 0.125 to 0.875 and a strain hardening coefficient of 1 to 20.

The elastic component of the J-integral for the equations of Lei et al. and Faucher corresponds with the one calculated using the formulas of Kumar (Eq. (4)). The difference lies in the method to calculate the plastic part of the J-integral. Lei et al. calculate the area between the load vs. CMOD curve and the secant offset line, $A_{p\delta}$, as shown in Figure 4. The equations by Faucher use the applied displacement (alternatively termed load line displacement or LLD) instead of the CMOD. This should approximate the value of the displacement due to plasticity at the crack zone. However, due to the high specimen length used in the simulations, the LLD is no longer representative for the plastic displacement at the crack as the contribution of linear elastic global specimen deformation becomes pronounced. This is especially the case for shallow cracks as plasticity is not only limited to the cross-section at the crack tip. Therefore, it was decided to use CMOD in an attempt to overcome this anomaly.

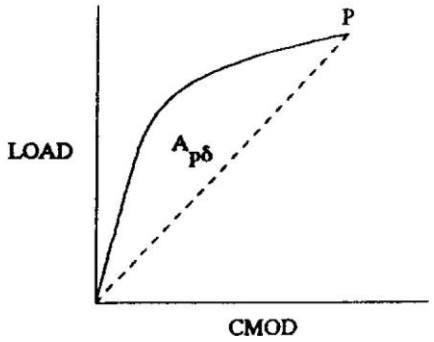

Figure 4. Definition of the area $A_{p\delta}$ by Lei et al. [10]

$$J_{pl} = \eta_{p\delta} \frac{A_{p\delta}}{B(W-a)} \tag{10}$$

The factor $\eta_{p\delta}$ is dependent on the strain hardening coefficient and the value of a/W. Values for CCT and DENT specimen geometries can be found for both plane stress and plane strain conditions (Faucher). Lei only has an $\eta_{p\delta}$ factor for CCT under plane strain conditions. The $\eta_{p\delta}$ factor is tabulated for specimens with a normalized crack depth of 0.125 to 0.875 and for a strain hardening coefficient of 2 to 20.

4 RESULTS

For both the CCT and DENT geometries, 3D and plane strain simulation results were compared to the analytical solutions. The thickness-width ratio B/W and the relative crack depth a/W were varied for both specimen geometries.

4.1 Center cracked tension (CCT)

The B/W ratio was varied between 0.1 and 1 for the 3D simulations and the plane strain simulations. 3D simulations were performed for a/W ratios of 0.25, 0.50 and 0.75. In Figure 5 an example of a typical CDF-curve of a CCT specimen is shown for a relative crack depth a/W of 0.75. Both the plane strain and plane stress analytical solutions according to the EPRI handbook are also shown in the figure as are the solutions by Faucher and Lei. The applied tensile force P has been normalized by the reference load P_0 of the plane stress condition (Kumar) to attain a more geometry independent result.

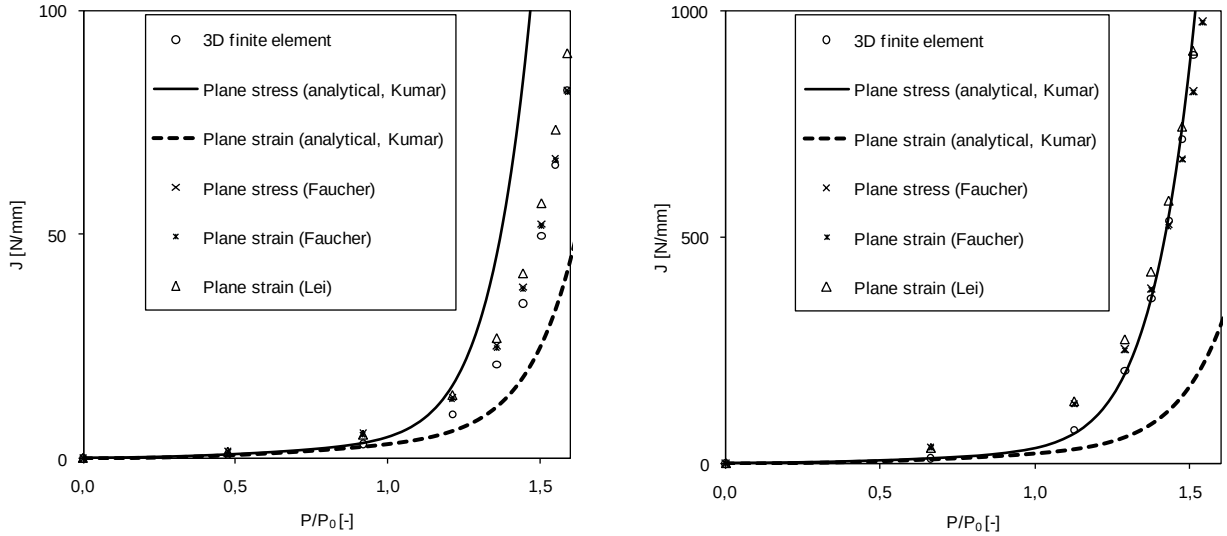

a) b)

Figure 5. 3D simulation CCT a) B/W=1, a/W=0.75. b) B/W=0.1 , a/W=0.75.

For the 3D simulations with B/W = 0.1 the CDF-curve almost coincides with the analytical solution for a plane stress condition. This was expected because a CCT specimen is known to closely approach the theoretical plane stress behaviour for low B/W values [13]. This is a good indication of the validity of the finite element model. The use of CMOD instead of LLD for the equations of Lei and Faucher is justified as it gives accurate results as can be seen in Figure 5.

To further justify the use of this model, the difference of the 3D simulation to the analytical solution for plane stress is calculated for different B/W ratio's. This is done by integrating the area between the normalized CDF curves of the simulation and the analytical solution for plane stress. The range of the integration is limited to an upper value of 1000 N/mm for the J-integral. Most experimental results for the J-integral are beneath this value. The resulting area is then divided by the area beneath the simulation curve. This allows to objectively quantify the discrepancy between both curves. The integration is done numerically with Simpson's rule. The difference between the simulation and the analytical result should decrease for lower B/W ratios. A thinner CCT specimen should approach the plane stress behaviour as the thickness is reduced. The differences are given in Table 1 to Table 3 as a function of the B/W ratio.

Table 1. Difference between 3D simulations and the analytical solutions for a/W=0.25 (CCT)

B/W	Difference plane stress (%)		Difference plane strain (%)		Difference Lei (%)
	Kumar	Faucher	Kumar	Faucher	
1.000	136.11	24.70	48.09	30.14	16.23
0.800	100.43	22.29	55.17	27.54	16.75
0.600	66.56	18.44	61.52	22.95	16.08
0.400	32.50	21.63	67.71	24.59	19.86
0.200	3.96	17.53	71.27	18.99	15.95
0.100	12.46	12.30	70.01	11.98	11.54

Table 2. Difference between 3D simulations and the analytical solutions for a/W=0.50 (CCT)

B/W	Difference plane stress (%)		Difference plane strain (%)		Difference Lei (%)
	Kumar	Faucher	Kumar	Faucher	
1.000	151.21	11.88	41.7	11.57	12.13
0.800	113.48	12.27	48.78	11.99	7.45
0.600	92.73	33.74	53.83	33.56	44.95
0.400	56.52	27.53	60.23	27.13	33.34
0.200	13.50	26.90	66.62	26.29	27.61
0.100	9.17	19.01	66.42	18.17	16.33

Table 3. Difference between 3D simulations and the analytical solutions for a/W=0.75 (CCT)

B/W	Difference plane stress (%)		Difference plane strain (%)		Difference Lei (%)
	Kumar	Faucher	Kumar	Faucher	
1.000	256.43	8.22	42.17	10.24	14.70
0.800	202.99	11.97	49.72	11.68	13.03
0.600	175.02	32.82	54.43	32.80	47.03
0.400	117.05	27.64	62.05	27.40	39.72
0.200	44.82	37.27	69.93	36.74	46.44
0.100	5.01	28.15	72.11	27.31	30.08

The finite element and the analytical solutions by Kumar for plane stress converge towards each other as the B/W ratio decreases, as is expected. The solution for plane strain on the other hand diverges from the 3D simultation. This further indicates the validity of the finite element model as the solutions composed by Kumar are purely analytical and are both limiting cases. The solutions by Lei and Faucher are more accurate analytical solutions because of the method used to calculate the plastic part of the J-integral. For that reason the solutions of Faucher and Lei closely resemble the simulated values as can be seen in the Tables 1 to 3 and Figure 5.

The value of the difference between 3D simulations and the analytical formula for plane stress according to Kumar for a specimen with B/W=0.1 and a/W=0.25 increases again with respect to the configuration B/W=0.2. This is caused by the intersecting of the simulations with the analytical curve for B/W=0.2 at higher loads and the simulation curve for B/W=0.1 lying slightly under the analytical curve. The difference for B/W=0.1 is therefore higher than for B/W=0.2 although the results approach the analytical values better. This problem is inherent of the method used to compare the finite element values to the analytical ones.

The discrepancy between the simulated plane strain values and the calculated theoretical values are given in Table 4. A performant finite element model should only allow little difference between the simulated values and the analytical solutions for plane strain conditions.

Table 4. Difference between plane strain simulations and the analytical plane strain solution (CCT)

B/W	Difference plane strain (%)		Difference Lei (%)
	Kumar	Faucher	
1.000	5.05	10.75	7.47
0.800	3.75	11.96	8.17
0.600	4.49	19.17	29.03
0.400	4.32	22.65	31.37
0.200	6.35	17.38	24.69
0.100	9.86	12.46	18.53

The differences between the finite element and the analytical values are small as can be seen in Figure 6. The value of the difference seems high, but that is caused by the length over which the curves are integrated.

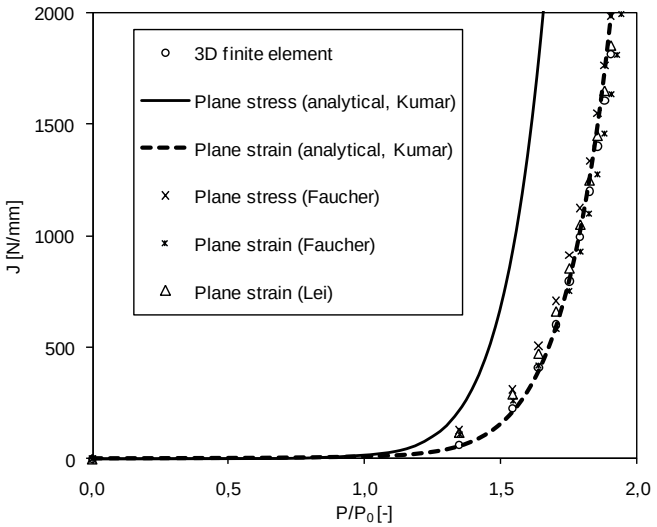

Figure 6. Plane strain simulation CCT, B/W=0.4 , a/W=0.25

4.2 Double edge notched tension

For the DENT specimen geometry, the same a/W, B/W and L/W ratios were used as for the CCT specimen. The results can be seen in Table 5 to Table 7. The same trends as for the CCT specimens can be discerned in the tables and are shown in Figure 7 for two B/W values.

Table 5. Difference between 3D simulations and the analytical solutions for a/W=0.25 (DENT)

B/W	Difference plane stress (%)		Difference plane strain (%)	
	Kumar	Faucher	Kumar	Faucher
1.000	88.66	14.70	68.87	20.64
0.800	47.33	23.08	72.02	27.11
0.600	28.47	22.88	76.67	27.91
0.400	11.11	21.19	78.15	26.15
0.200	12.82	21.36	78.31	26.40
0.100	26.59	21.04	75.57	25.25

Table 6. Difference between 3D simulations and the analytical solutions for a/W=0.50 (DENT)

B/W	Difference plane stress (%)		Difference plane strain (%)	
	Kumar	Faucher	Kumar	Faucher
1.000	245.77	13.17	73.84	35.94
0.800	172.14	13.34	77.11	35.99
0.600	112.78	19.55	81.07	37.80
0.400	51.96	21.33	82.73	39.74
0.200	9.38	27.34	80.67	38.88
0.100	8.97	17.06	74.04	35.86

Table 7. Difference between 3D simulations and the analytical solutions for a/W=0.75 (DENT)

B/W	Difference plane stress (%)		Difference plane strain (%)	
	Kumar	Faucher	Kumar	Faucher
1.000	2691.18	17.98	73.39	33.45
0.800	1833.96	16.64	79.07	34.60
0.600	1051.54	17.27	85.07	37.51
0.400	366.16	20.26	87.98	39.83
0.200	84.55	43.99	85.48	44.45
0.100	20.74	19.63	78.81	37.23

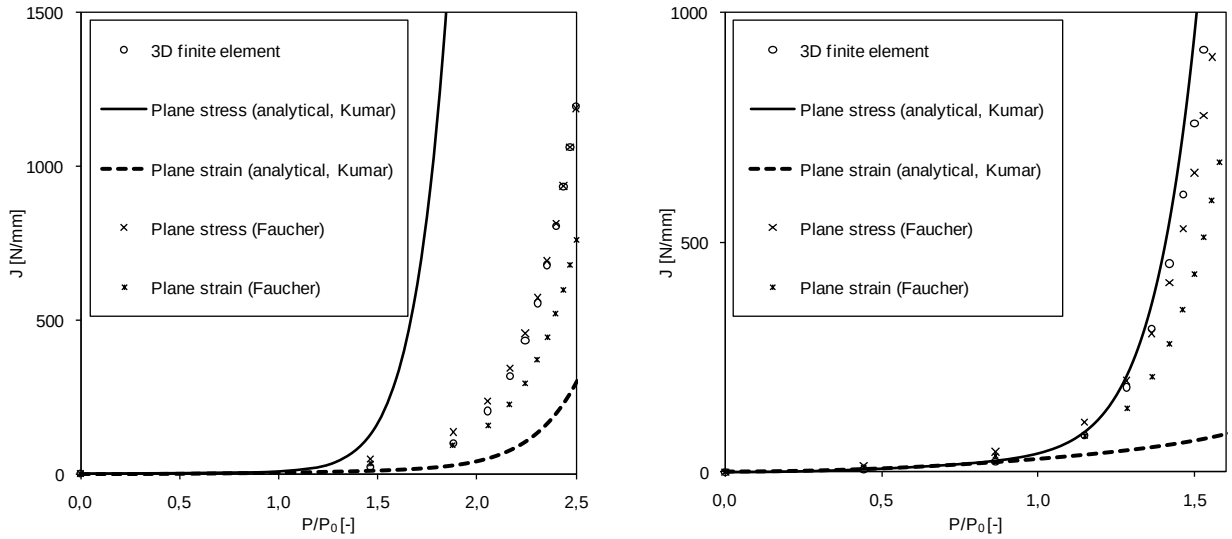

Figure 7. 3D simulation DENT a) B/W=1, a/W=0.75. b) B/W=0.1 , a/W=0.75

In Table 8 the difference between a plane strain simulation and the analytical results can be seen. The simulations approach the analytical plane strain solutions by Kumar as can be seen in Figure 8.

Table 8. Difference between plane strain simulations and the analytical plane strain solution (DENT)

B/W	Difference plane strain (%)	
	Kumar	Faucher
1.000	19.00	14.23
0.800	19.51	13.41
0.600	16.66	19.00
0.400	21.18	12.89
0.200	22.00	14.27
0.100	23.96	13.31

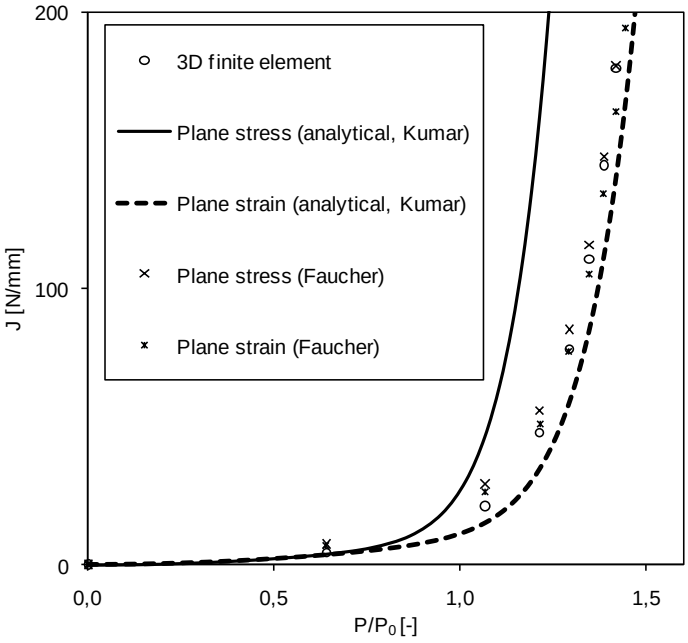

Figure 8. Plane strain simulation DENT, B/W=0.4 , a/W=0.25

5 CONCLUSIONS

The finite element model has proven accuracy for the calculation of J-integral values for fracture mechanics standardized specimens, such as CCT and DENT. Both the 3D and 2D plane strain simulations give representative values as compared to known analytical solutions. As a conclusion, the model can be confidently used to determine values of the J-integral. This is a first step towards evaluating two parameter J-Q constraint.

6 NOMENCLATURE

J	J-integral	N/mm
J_e	elastic part of the J-integral	N/mm
J_p	plastic part of the J-integral	N/mm
J_0	normalizing factor J-integral	N/mm
σ	stress	MPa
ε	strain	-
σ_0	yield stress	MPa
ε_0	yield strain	-
E	Young's modulus	MPa
n	strain hardening coefficient	-
K_I	stress intensity factor, mode I	MPa$\sqrt{m}$
P	tensile force	N
P_0	normalized tensile force	N
ν	Poisson's ratio	-
a	crack depth	mm
B	specimen thickness	mm
W	specimen width	mm
L	Specimen length	mm
b	half of the remaining ligament	mm

7 ACKNOWLEDGEMENTS

The authors would like to acknowledge the financial support of the IWT (Agency for innovation by science and technology – grant n° SB-091512 and SB-093512) and the FWO (Research Foundation Flanders – grants n° 1.1.880.09.N.00, 1.1.880.11.N.01 and 1.5.247.08N.00).

8 REFERENCES

[1] Dogan B., Nikbin K., Petrovski B., Ceyhan U., Dean D.W., Code of practice for high-temperature testing of weldments, International Journal of Pressure Vessels and Piping, Volume 83, Issues 11-12, November-December 2006, Pages 784-797

[2] Gengenbach, T. and Klenk, A., Creep, Creep-fatigue Crack Initiation and Growth in 9-12% Chromium Steels., OMMI, Vol. 3, 2004.

[3] Knockaert, R., Doghri, I., Marchal, Y., Pardoen, T. and Delannay, F., Experimental and Numerical Investigation of Fracture in Double-edge Notched Steel Plates, International Journal of Fracture 81, pp. 383-399, 1996.

[4] Liu, C.H., Mang, H.A., Chen, D.L., Weiss, B. and Stickler, R., Numerical Assessment of Stress Distribution Ahead of the Crack Tip for Finite-Width Center Cracked Tension Specimen, International Journal of Fracture 63: R67-R74, 1993.

[5] Francis, M. and Rahman, S., Probabilistic Analysis of Weld Cracks in Center-cracked Tension Specimens, Computers and Structures 76, pp. 483-506, 2000.

[6] Goldman, N.L. and Hutchinson, W., Fully Plastic Crack Problems: the Center-cracked Stip under Plane Strain, Int. J. Solids Structures, Vol. 11, pp. 575-591, 1975.

[7] Dogan, B., Nikbin, K. and Petrovski B., Development of European creep crack growth testing code of practice for industrial specimens, EPRI Int. Conf "Materials and Corrosion Experience for Fossil Power Plants".

[8] Schwalbe, K., Neale, B. and Heerens, J., The GKSS test procedure for determining the fracture behaviour of materials, *EFAM GTP*, vol. 94, 1994.

[9] Kumar, V., German, M.D., and Shih, C.F.,"An Engineering Approach for Elastic-Plastic Fracture Analysis." EPRI Report NP-1931, Electric Power Research Institute, Palo Alto, CA, 1981.

[10] Lei, Y. and Neale, B.K., The Fracture Behavious of a Centre Cracked Tensile Specimen, Fatigue and Fracture of Engineering Materials and Structures, Vol. 20, No. 2, pp. 201-216, 1997.

[11] Faucher, B., Crack length and J-integral Expressions for Specimens Loaded in Tension, Journal of Testing and Evaluation, JTEVA, Vol. 22, No. 1, pp. 30-35, January 1994.

[12] Anderson, T.L.. Fracture Mechanics: Fundamentals and Applications 2nd edition, CRC Press, 1995.

[13] Kim, Y.-J. and Schwalbe, K.-H., On the Sensitivity of J Estimation to Materials' Stress-Strain Curves in Fracture Toughness Testing Using the Finite Element Method, Journal of Testing and Evaluation, JTEVA, Vol. 29, No. 1, January 2001, pp. 18–30.